ST-ECF Instrument Science Report WFC3-2008-15

The TV2 ground calibrations of the WFC3 NIR grisms

H. Kuntschner, H. Bushouse, J. R. Walsh, M. Kümmel
July 08, 2008

ABSTRACT

Based on thermal vacuum tests (TV2; June - August 2007), the performance of the WFC3 near-IR G102 and G141 grisms has been assessed. The locations of the different orders relative to exposures taken through a direct imaging filter are determined, trace and wavelength solutions are derived, and the absolute throughput of the different orders is quantified. The trace and wavelength solutions were found to be linear functions varying smoothly as function of field of view. Aperture corrections are given for both grims as function of wavelength. Furthermore, we describe flat-field cubes that provide pixel-to-pixel information as function of wavelength to an accuracy of about 1%.
New detectors in the UV and IR channels are being tested in TV3 (March – April 2008), therefore updates for the sensitivity calibrations are to be expected while geometric properties are predicted to remain stable.

1. Introduction

The Wide Field Camera 3 (WFC3) is fitted with three grisms for slitless spectroscopy. In the UVIS channel there is one grism, G280, for the near-UV to visible range (200 - 400nm). The NIR channel has two grisms (G102 and G141) for the shorter (800 - 1150nm) and longer NIR wavelengths (1100-1700nm).

The fundamental design parameters of a grism are the deflection of the incident beam by the grism (defined by the prism angle), the dispersion in the various orders and the energy in each order (defined by the groove frequency and profile). In order to extract slitless spectra from grism images it is necessary to know these parameters and their variation with position in the field. With a good parameterization, then extraction software, such as the aXe tasks developed at the ST-ECF (http://www.stecf.org/software/slitless_software/), can be applied to extract multiple slitless spectra from sky images in a semi-automatic fashion. A further use of the parameterization is to provide a simulation package which can predict two-dimensional dispersed images of a given sky region if an input catalogue is provided. The ST-ECF has developed such a package (aXeSIM; Kümmel, Kuntschner, Walsh 2007), which was available to the Cycle 17 proposal deadline.

During the Thermal Vacuum testing of WFC3 in June - August 2007 (TV2), specific calibrations for the grisms were included. The tests were designed to allow determination of the spectral trace, the dispersion solution and the absolute instrument throughput by using a combination of monochromator and white light source measurements. Additionally, the detector flat-field was determined with 10nm wide bandpasses in steps of 20nm. This ISR describes the implementation of the tests and the analysis of the results. Tables provide the details of the field position dependent spectral trace and the dispersion solutions for the two IR-channel grisms; measurements of the total instrument throughput and information on the wavelength dependent flat-field are also provided.

This instrument science report (ISR) is a follow up on the report by Larsen, Bushouse, & Walsh (WFC3-2005-07) from the TV1 calibrations.

2. Calibration set-up for TV2

The grism test procedures were executed during June - August 2007, with the WFC3 in a flight-like thermal-vacuum environment. The WFC3 external optical stimulus system, CASTLE, was used to provide the necessary source targets for the tests. For these tests, the WFC3 IR detector (IR1 “FPA129”) was at an operating temperature of -123°C and the IR Filter Select Mechanism (FSM) was at a temperature of -42°C. The IR16S30 series and IR16S40 series test procedures use sets of point-source exposures, all of which were obtained with the CASTLE quartz-tungsten-halogen (QTH) lamp, and a 10 micron pinhole to provide an unresolved target, which is used to determine the dispersion solution and spectral trace for each grism. The IR14S13 and IR14S14 test procedures use an extended source (200 micron pinhole) to provide high S/N photometric measurements of the absolute instrument throughput with the grisms in place.

3. Calibration measurements

For each IR grism calibration measurements were carried out to allow determination of the spectral trace, the dispersion solution and the absolute instrument throughput as well as a wavelength dependent flat-field. A summary of all NIR grism calibration procedures is given in Table 1. Absolute throughput is determined for a central position only, while trace and dispersion calibrations are performed in a 5-point pattern (center and the four quadrants) to allow for a 2-dim solution covering the full field-of-view. Figure 1 shows graphically the distribution of the individual pointings. Since the 1st order spectrum is located to the right of the direct image position (see also Figures 2 and 3), the point source positions are not centered on the detector but shifted towards smaller x-axis values.

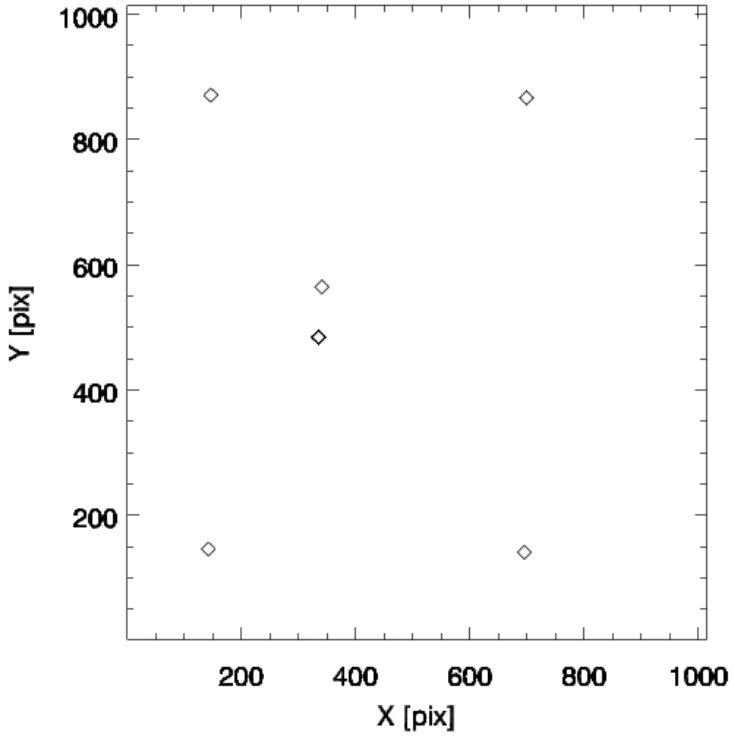

Figure 1: Distribution of the point source positions for the G102 trace and wavelength calibrations. The setup for G141 is identical. Quadrants as noted in Table 1 are counted such that Quadrant 1 is in the upper left corner and then numbers increase anti-clockwise.

Table 1. Summary of NIR grism calibrations

Test procedure	Date	Grism	Purpose
IR14S11	**2007-07-15**	**G102**	**Flat-field**
IR14S12	**2007-07-16**	**G141**	**Flat-field**
IR14S13	**2007-07-27**	**G102**	**Absolute throughput**
IR14S14	**2007-07-27**	**G141**	**Absolute throughput**
IR16S30	**2007-07-06**	**G102**	**Dispersion (center)**
IR16S30	**2007-08-20**	**G102**	**Dispersion (center) - repeat**
IR16S31	**2007-08-20**	**G102**	**Dispersion (quadrant 1)**
IR16S32	**2007-08-20**	**G102**	**Dispersion (quadrant 2)**
IR16S33	**2007-08-20**	**G102**	**Dispersion (quadrant 3)**
IR16S34	**2007-08-20**	**G102**	**Dispersion (quadrant 4)**
IR16S40	**2007-07-06**	**G141**	**Dispersion (center)**
IR16S40	**2007-08-20**	**G141**	**Dispersion (center) - repeat**
IR16S41	**2007-08-20**	**G141**	**Dispersion (quadrant 1)**
IR16S42	**2007-08-20**	**G141**	**Dispersion (quadrant 2)**
IR16S43	**2007-08-20**	**G141**	**Dispersion (quadrant 3)**
IR16S44	**2007-08-20**	**G141**	**Dispersion (quadrant 4)**

The absolute throughput measurements were carried out with a calibrated monochromator source covering for the G102 grism the range 780nm - 1180nm in steps of 20nm; and for the G141 grism the range 1040nm – 1700nm in steps of 20nm. After the calibrations were carried out, corrections to the effective gain and neutral density filters became known (September 2007). All results presented in this report are using a gain value of 2.4 and the correction factors for the stimulus flux (OSFLUX keyword) were applied.

The trace and dispersion calibrations were carried out starting with a set of three direct image and grism pairs using a white light stimulus. After that monochromator steps covering for the G102 grism the range 760nm - 1180nm in steps of 20nm; and for the G141 grism the range 1000nm – 1700nm in steps of 50nm, were performed. In all cases, the monochromator bandwidth was 10 nm.

Additionally, the detector flat-field was determined with 10nm wide bandpasses in steps of 20nm, covering for the G102 grism the range 780nm - 1180nm; and for the G141 grism the range 1060nm – 1700nm.

4. Analysis

In this section we describe the analysis of the calibration data yielding calibrations for the trace, wavelength and absolute throughput.

4.1. Trace calibration

The ST-ECF aXe package for reduction of slitless spectroscopy data treats the spectral traces and wavelength solutions defined with respect to the position of the source in the direct image. The centroids of the continuum source images in the direct imaging exposures (X_{ref}, Y_{ref}) were determined with the IRAF task imexam. These positions were assumed not to change through the duration of the remaining measurements. The continuum lamp spectra (see also Figure 2 and 3) were traced as a function of $\Delta X=X-X_{ref}$ in the detector X-direction by measuring the centroids of 5-7 pixel wide bins, using custom-written IDL programs. We found the traces of all orders (excluding the zeroth order) to be well fit by straight lines with standard deviations of $\leq$ 0.07 pixels. The trace definitions are of the form $(Y-Y_{ref})$=DYDX_0 + DYDX_1*ΔX, where DYDX_0 and DYDX_1 are field dependent and given in the usual format used by the ST-ECF aXe reduction package, e.g., DYDX_1 = a0 +a1*X_{ref} + a2*Y_{ref} + …(see also aXe manual for more details). The coefficients of our field dependent fits are given in Table 2 and 3 for the G102 and G141 grisms, respectively. Given the sparse sampling of the field-of-view (see Figure 1) only linear terms are considered in the field dependent fits.

With an accuracy of better than one pixel the traces of the orders are collinear. We also derive trace solutions for the 0^{th} order, however, these are only approximate, and hence meaningful errors estimates could not be derived (see Tables 2 and 3).

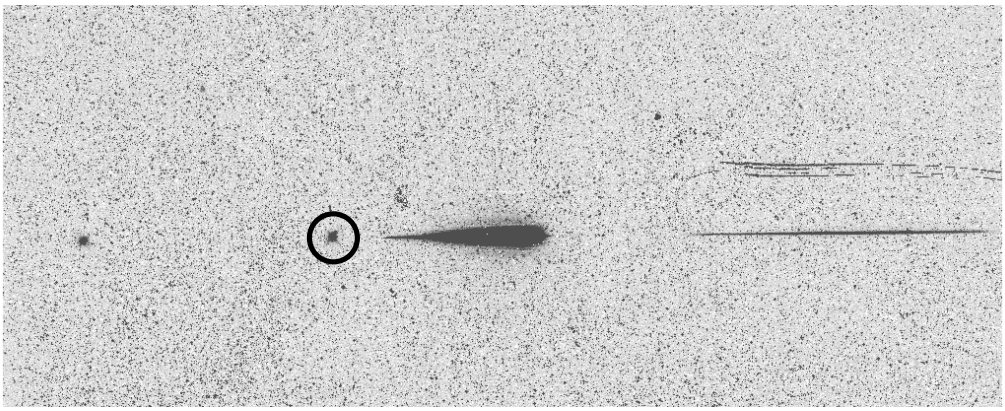

Figure 2: Sum of a direct image (F105W) and a G102 exposure of the continuum source. A circle marks the location of the source in the direct image, and the grism $+1^{st}$ and $+2^{nd}$ orders can be seen extending towards the right. The grism 0^{th} order is also visible as a point source like feature to the left of the direct image. The full extent of the detector (1014 pixels) is shown in x-direction. Several "strips" of bad pixels are visible just above the second order.

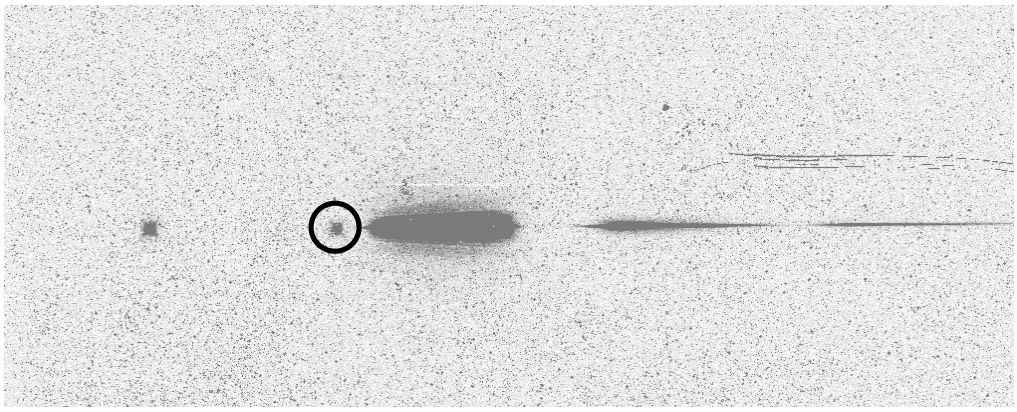

Figure 3: Sum of a direct image (F139W) and a G141 exposure of the continuum source. A circle marks the location of the source in the direct image, and the grism +1st, +2nd and +3rd orders can be seen extending towards the right. The grism 0th order is again visible as a point source like feature to the left of the direct image.

Table 2: Field dependent trace descriptions for G102. Errors are given in brackets.

Term	a0	a1(X)	a2(Y)
+1st order			
DYDX_A_0	-6.2287E-01 (8.9206E-02)	9.7066E-05 (1.8662E-04)	-1.4220E-03 (1.4483E-04)
DYDX_A_1	9.3587E-03 (8.4666E-04)	1.6237E-07 (1.7712E-06)	3.6163E-06 (1.3746E-06)
0th order			
DYDX_B_0	-3.6549E+00	8.4494E-04	-1.1890E-03
DYDX_B_1	0.0	-	-
XOFF_B	-2.5918E+02	-1.7154E-03	1.5011E-02
+2nd order			
DYDX_C_0	5.4198E-01 (4.6494E-02)	-6.5235E-04 (2.7063E-04)	-3.4318E-03 (1.1598E-04)
DYDX_C_1	8.0690E-03 (7.4165E-05)	-1.0805E-06 (4.3170E-07)	5.3395E-06 (1.8500E-07)

Table 3: Field dependent trace descriptions for G141. Errors are given in brackets.

Term	a0	a1(X)	a2(Y)
$+1^{st}$ order			
DYDX_A_0	1.9770E+00 (7.0509E-02)	4.7900E-05 (1.4747E-04)	-1.8890E-03 (1.1442E-04)
DYDX_A_1	4.9871E-03 (9.3977E-04)	8.7047E-07 (1.9655E-06)	4.3156E-06 (1.5250E-06)
0^{th} order			
DYDX_B_0	6.5863E-01	1.5840E-04	-1.6251E-03
DYDX_B_1	0.0	-	-
XOFF	-1.9224E+02	-2.3144E-03	1.1109E-02
$+2^{nd}$ order			
DYDX_C_0	2.2577E+00 (5.8889E-02)	1.6404E-04 (1.2317E-04)	-3.0160E-03 (9.5561E-05)
DYDX_C_1	3.6282E-03 (1.1997E-03)	2.6386E-07 (2.5092E-06)	6.9699E-06 (1.9468E-06)
$+3^{rd}$ order			
DYDX_D_0	2.1320E+00 (7.3501E-02)	2.9334E-04 (4.2827E-04)	-2.7934E-03 (1.8324E-04)
DYDX_D_1	5.9995E-03 (2.1223E-04)	-5.6133E-07 (1.2366E-06)	2.4976E-06 (5.2910E-07)

4.2. Wavelength solutions

The trace definitions derived in Section 4.1 were inserted into a configuration file for the spectral extraction software (aXe) and each of the monochromator spectra were then extracted using the standard aXe task AXECORE. The software automatically extracts the spectral orders as separate "beams", defined with respect to the location of the object in the direct image. The FITS files produced by aXe were then analyzed by custom built IDL scripts where the (X-Xref) location of the peak of each monochromator spot was measured by fitting a Gaussian.

The wavelength solutions were found to be well approximated by linear fits to wavelength versus pixel offset. For G102 the standard deviation around the linear fit was typically 2 Å for the 1st order (dispersion ~25 Å/pixel) and 3-4 Å for the second order (dispersion ~12 Å/pixel). For G141 the standard deviation around the linear fit was typically 2 Å for the 1st order (dispersion ~47 Å/pixel) and 1-3 Å for

the second order (dispersion ~23 Å/pixel). Within the uncertainties, the wavelength solutions behave as expected, with the +1st and -1st orders having similar dispersions, and the +2nd and +3rd orders having dispersions of 1/2 and 1/3 of that of the 1st order. The 0th order spectra also show a small dispersion. We do not characterize the 3rd order for G102 since it is mostly outside the detector area for the available pointings.

Similar to the trace solutions, the dispersion solutions also show variations across the field of view that can be approximated by linear fits. For example, for the G102 grism (1st order), the dispersion varies from 24.0 to 25.8 Å/pixel across the field of view mostly as function of y-axis position, while for the G141 grism it varies from 45.5 to 48.0 Å/pixel. The coefficients of our field dependent fits are given in Table 4 and 5 for the G102 and G141 grisms, respectively.

Table 4: Field dependent dispersion descriptions for G102. Errors are given in brackets.

Term	a0	a1(X)	a2(Y)
+1st order			
DLDP_A_0	6.3571E+03 (7.1589E-01)	5.3489E-02 (1.6472E-03)	3.9486E-03 (1.2695E-03)
DLDP_A_1	2.3924E+01 (1.2344E-02)	-1.3224E-04 (2.8403E-05)	1.4786E-03 (2.1891E-05)
0th order			
DLDP_B_0	1.0436E+04 (1.8076E+02)	-1.3314E+00 (8.7153E-01)	5.2446E-01 (6.0628E-01)
DLDP_B_1	1.3707E+03 (1.3176E+02)	-5.5924E-01 (6.3526E-01)	5.3204E-01 (4.4192E-01)
+2nd order			
DLDP_C_0	3.2105E+03 (1.0574E+00)	8.8933E-02 (9.4755E-03)	-1.3463E-02 (3.5520E-03)
DLDP_C_1	1.2058E+01 (7.9651E-04)	-2.0007E-04 (7.1378E-06)	7.7748E-04 (2.6757E-06)

Table 5: Field dependent dispersion descriptions for G141. Errors are given in brackets.

Term	a0	a1(X)	a2(Y)
+1st order			
DLDP_A_0	8.9124E+03 (3.0080E+00)	1.0482E-01 (6.9200E-03)	9.1073E-03 (5.3318E-03)
DLDP_A_1	4.5312E+01 (3.0552E-02)	-2.0978E-04 (7.0284E-05)	2.8211E-03 (5.4153E-05)
0th order			
DLDP_B_0	1.3220E+04 (3.4769E+01)	-7.5031E-01 (1.6754E-01)	-1.7850E-01 (1.1657E-01)
DLDP_B_1	2.3240E+03 (1.6974E+02)	-	-
+2nd order			
DLDP_C_0	4.5015E+03 (5.8268E+00)	1.6366E-01 (5.2257E-02)	-6.8672E-02 (1.9562E-02)
DLDP_C_1	2.2829E+01 (1.3558E-02)	-4.1939E-04 (1.2159E-04)	1.6253E-03 (4.5518E-05)
+3rd order			
DLDP_D_0	3.0548E+03 (3.5218E+00)	-3.0712E-04 (3.1585E-02)	2.7126E-02 (1.1824E-02)
DLDP_D_1	1.5183E+01 (3.5142E-03)	-4.2190E-05 (3.1516E-05)	8.9823E-04 (1.1798E-05)

4.3. Absolute throughput calibrations

For each of the calibrated monochromator settings (see also Section 3) and all visible orders, the detected counts were measured with the IRAF task imexam. The aperture radius was adjusted with 3 iterations generally resulting in radii of about 17 pixel. The ratio of detected flux (using a gain of 2.4 e/DN) versus the incoming flux as recorded in the image headers (keyword OSFLUX, given as flux per second) gives then the instrument efficiency. Figures 4 and 5 present the efficiency curves for WFC3 with the G102 and G141 grisms, respectively. The plots show the efficiency of WFC3 as measured in TV2 but do not include any contributions from the OTA throughput.

For G102, the peak efficiency of ~31% is reached between 1020 and 1120nm in the +1st order. Efficiency above 10% is achieved over a broad wavelength range from 820 to 1140nm. Due to the excellent design of the grism, the throughput in the +2nd

and zeroth order is much lower with a maximum of 4.4 and 1.4%, respectively.

For G141, the peak efficiency of ~41% is reached between 1440 and 1640nm in the $+1^{st}$ order. Efficiency above 10% is achieved over a broad wavelength range from 1100 to 1680nm, thus giving continuous wavelength coverage from 820 to 1680nm with the two grisms together. Due to the excellent design of the G141 grism, the throughput in the $+2^{nd}$, 3^{rd} and zeroth order is much lower with a maximum of 6, 0.5 and 1.4%, respectively.

Tables 6 and 7 present the efficiency measurements in tabular form for the G102 and G141 grisms, respectively.

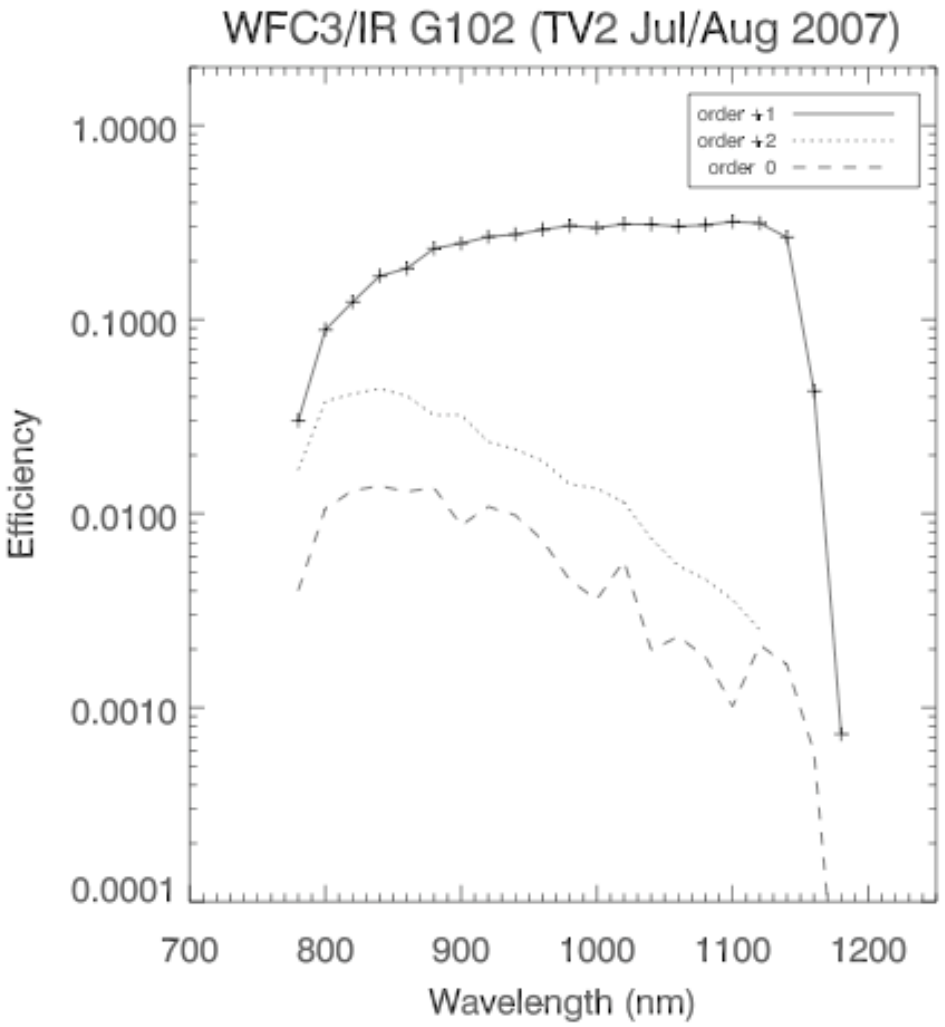

Figure 4: Instrument efficiency of various orders for the WFC3 G102 grism as function of wavelength.

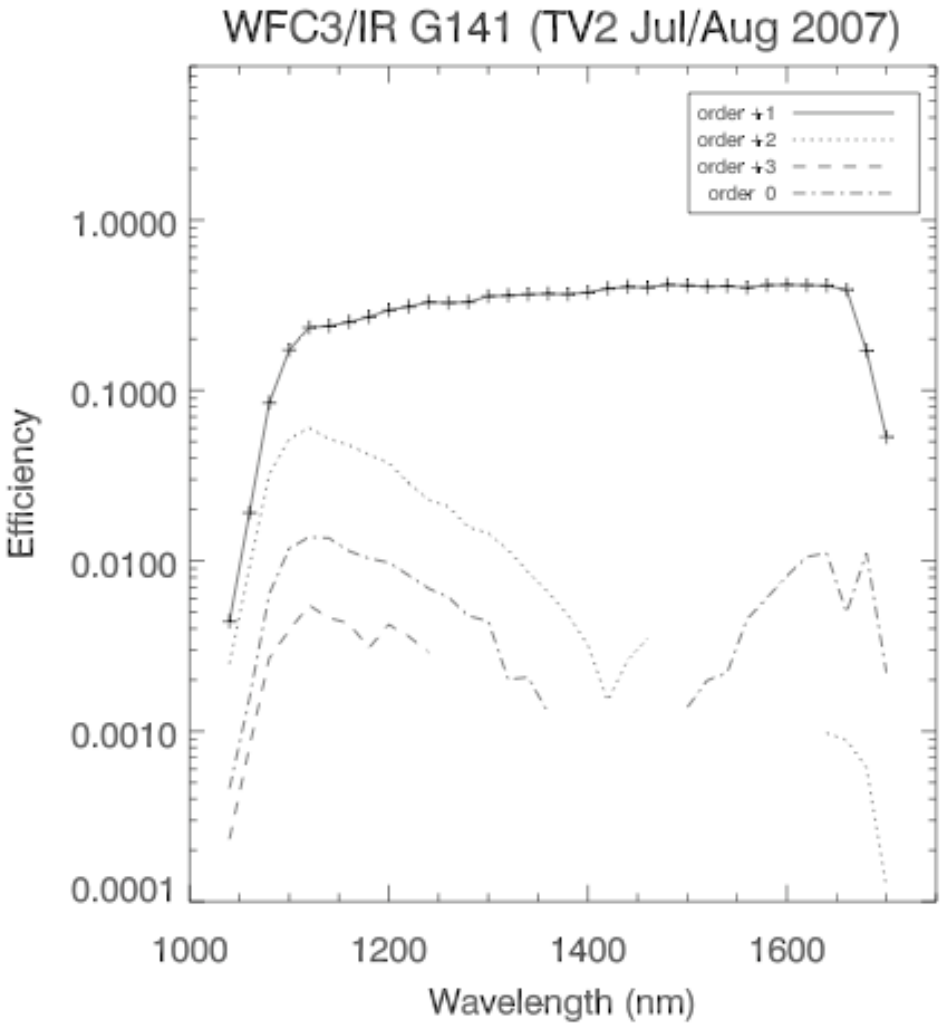

Figure 5: Instrument efficiency of various orders for the WFC3 G141 grism as function of wavelength. The wavelength coverage is interrupted for 0^{th} and 2^{nd} orders on account of insufficient signal.

Table 6: Instrument efficiency for WFC3 G102

Wavelength (nm)	0th order	1st order	2nd order
7800	0.0040	0.0301	0.0169
8000	0.0106	0.0886	0.0379
8200	0.0131	0.1232	0.0414
8400	0.0139	0.1676	0.0441
8600	0.0130	0.1835	0.0404
8800	0.0136	0.2323	0.0322
9000	0.0087	0.2469	0.0323
9200	0.0109	0.2670	0.0234
9400	0.0098	0.2747	0.0215
9600	0.0073	0.2908	0.0187
9800	0.0045	0.3043	0.0142
10000	0.0036	0.2969	0.0135
10200	0.0057	0.3107	0.0114
10400	0.0020	0.3089	0.0075
10600	0.0023	0.3021	0.0054
10800	0.0018	0.3068	0.0046
11000	0.0010	0.3193	0.0036
11200	0.0021	0.3136	0.0025
11400	0.0017	0.2656	-
11600	0.0006	0.0427	-
11800	-	0.0007	-

Table 7: Instrument efficiency for WFC3 G141

Wavelength (nm)	0th order	1st order	2nd order	3rd order
10400	0.0005	0.0044	0.0025	0.0002
10600	0.0016	0.0191	0.0091	0.0008
10800	0.0064	0.0846	0.0322	0.0027
11000	0.0118	0.1724	0.0519	0.0039
11200	0.0138	0.2343	0.0604	0.0055
11400	0.0136	0.2386	0.0519	0.0046
11600	0.0114	0.2516	0.0477	0.0043
11800	0.0103	0.2697	0.0420	0.0031
12000	0.0098	0.2957	0.0376	0.0042
12200	0.0082	0.3097	0.0286	0.0036
12400	0.0069	0.3291	0.0228	0.0029
12600	0.0061	0.3266	0.0208	-
12800	0.0047	0.3297	0.0157	-
13000	0.0044	0.3571	0.0145	-
13200	0.0020	0.3603	0.0116	-
13400	0.0021	0.3665	0.0086	-
13600	0.0013	0.3691	0.0066	-
13800	-	0.3669	0.0048	-
14000	-	0.3760	0.0032	-
14200	-	0.3956	0.0015	-
14400	-	0.4051	0.0026	-
14600	-	0.4019	0.0035	-
14800	-	0.4168	-	-
15000	0.0014	0.4127	-	-
15200	0.0020	0.4067	-	-
15400	0.0022	0.4094	-	-
15600	0.0045	0.4011	-	-
15800	0.0061	0.4147	-	-
16000	0.0082	0.4167	-	-
16200	0.0106	0.4148	-	-
16400	0.0111	0.4119	0.0010	-
16600	0.0050	0.3899	0.0009	-
16800	0.0111	0.1711	0.0006	-
17000	0.0022	0.0533	0.0001	-

4.4. Aperture corrections

Aperture corrections were derived for both near-IR grims by using the aXe software to extract a rectified 2-dim image around a continuum exposure. The resulting image (called "stamp" image) is wavelength calibrated and image distortions as recorded in our trace calibrations are removed. From this image covering a large region around the continuum exposure various sub-apertures (here used in the sense of a diameter) are extracted with the help of IDL scripts and compared to the flux one determines in the largest aperture. This procedure is carried out as function of wavelength in six bins for each grism. The resulting aperture correction values are given in Tables 8 and 9 for the G102 and G141 grisms, respectively.

For both grisms about 95% of the flux is concentrated in an aperture (=diameter) of about 15 pixels or 1.95 arcsec.

Table 8: Aperture corrections for WFC3 G102

Aperture [pixel]	8850 Å	9350 Å	9850 Å	10350 Å	10850 Å	11350 Å
1	0.432	0.364	0.376	0.450	0.438	0.385
3	0.791	0.787	0.786	0.800	0.800	0.791
5	0.859	0.868	0.872	0.871	0.876	0.883
7	0.889	0.901	0.902	0.901	0.906	0.914
9	0.913	0.924	0.925	0.925	0.928	0.937
11	0.932	0.939	0.941	0.940	0.944	0.953
13	0.943	0.950	0.951	0.950	0.955	0.963
15	0.952	0.957	0.959	0.959	0.964	0.970
29	0.974	0.977	0.979	0.979	0.984	0.987
59	0.991	0.990	0.991	0.991	0.996	0.995
101	0.997	0.996	0.996	0.996	0.999	0.998
201	1.000	1.000	1.000	1.000	1.000	1.000

Table 9: Aperture corrections for WFC3 G141

Aperture [pixels]	11300 Å	12300 Å	13300 Å	14300 Å	15300 Å	16300 Å
1	0.394	0.388	0.347	0.313	0.296	0.295
3	0.772	0.760	0.723	0.698	0.698	0.698
5	0.867	0.850	0.835	0.834	0.838	0.837
7	0.897	0.878	0.871	0.874	0.876	0.880
9	0.920	0.904	0.900	0.897	0.899	0.903
11	0.936	0.926	0.920	0.916	0.918	0.921
13	0.947	0.939	0.935	0.933	0.933	0.936
15	0.955	0.948	0.945	0.944	0.945	0.949
29	0.978	0.976	0.977	0.977	0.980	0.981
59	0.990	0.990	0.991	0.991	0.993	0.993
101	0.996	0.997	0.997	0.997	0.998	0.997
201	1.000	1.000	1.000	1.000	1.000	1.000

4.5. Flat-field determinations

In slitless spectroscopy each pixel can receive any wavelength in the range of the grism, so it is necessary to build a flat-field cube in order to assign a flat-field correction for all pixels and wavelengths. The aXe reduction software employs a flat-field cube in the form of a polynomial fit to the wavelength variation of the flat-field. The input data for constructing a flat-field cube are thus a set of flat-fields at specified wavelengths. Using CASTLE and the monochromator the G102 and G141 grisms were illuminated with light over the relevant wavelength range of each grism: for G102 8000 to 11800Å in steps of 200Å; for G141 10600 to 17000Å, also in steps of 200Å. The monochromator slit was set to produce light of wavelength width 100Å.

Figure 6 shows the G102 image at 10000 Å. There is a modest (~20%) illumination pattern increasing from left to right and bottom to top, which was common to all the exposures for both grisms. This was removed by fitting a surface using the IRAF task **imsurfit**. It was found that the illumination is rather flat to the right of column 300 so better fits could be obtained by splitting the image at row 300 and separately performing the surface fits for these two sections, then combining the results. A spline was used for the fitting function with order 5 in X and order 12 in Y for both grisms. Figure 7 shows the resulting flat-field for G102 at 10000Å. Only the G102 flat is shown here; the G141 flat-field images are very similar in appearance. The sets of flat-fields were fitted pixel-by-pixel with wavelength to

produce the flat-field cubes. A 3rd order polynomial was found to be adequate and the residual images on the fit showed mean values of 1.2 and 0.8% for the G102 and G141 grisms, respectively. As demonstration of the wavelength dependence of the flat-fields, Figure 8 shows examples for a few selected pixels. Two pixels lying at the mean flat-field response of 1.0 are show in blue and red, as representative of the majority of the pixels. The green points show the wavelength dependence for a 'high' pixel and the magenta points for a 'low' pixel. The open circles show the points generated from the polynomial fit.

One of the reasons for using monochromatic light with width 100Å was to investigate any possible fringing with wavelength of the detector. Comparing images at different wavelengths, no evidence for fringing to a level of about 1% was seen. This is also apparent from the plots on Figure 8 where the flat-field behaviour is rather flat with wavelength, even for the high and low response pixels.

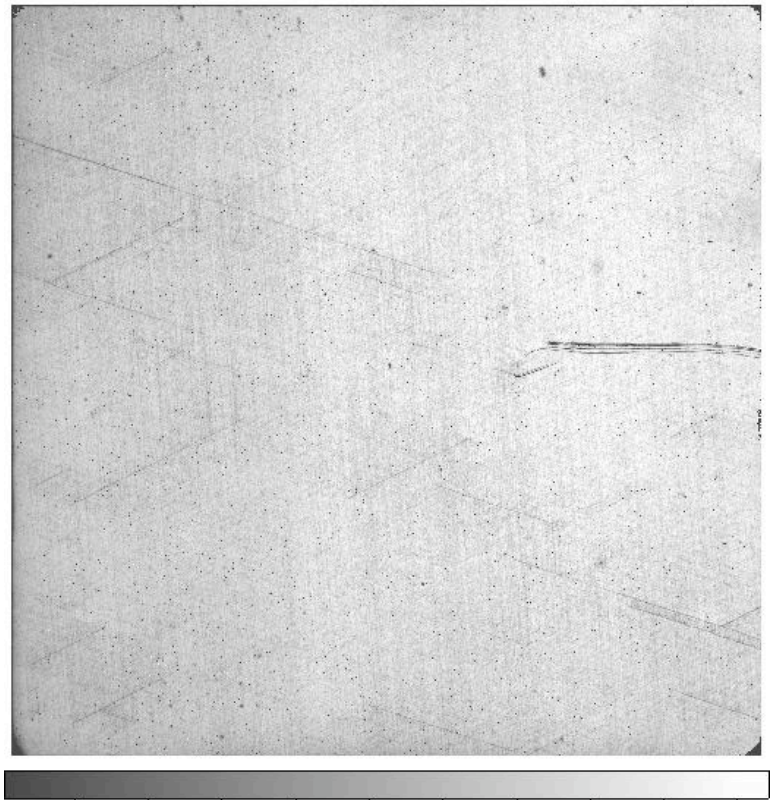

Figure 6: Example of the monochromatic image at 10000Å taken with the G102 grism. The mean level is 8500 ADU and the greyscale range is mean 3600 - 10150 (black - white).

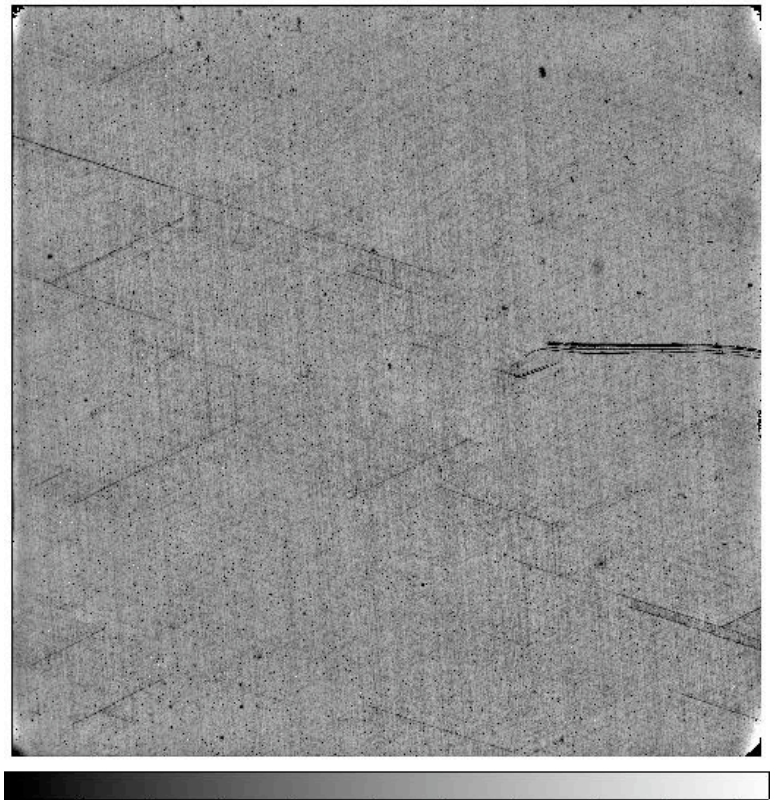

Figure 7: The resulting normalised flat-field image for the G102 grism at 10000Å, derived from the image shown in Figure 6. The greyscale is -/+ 33% about the mean.

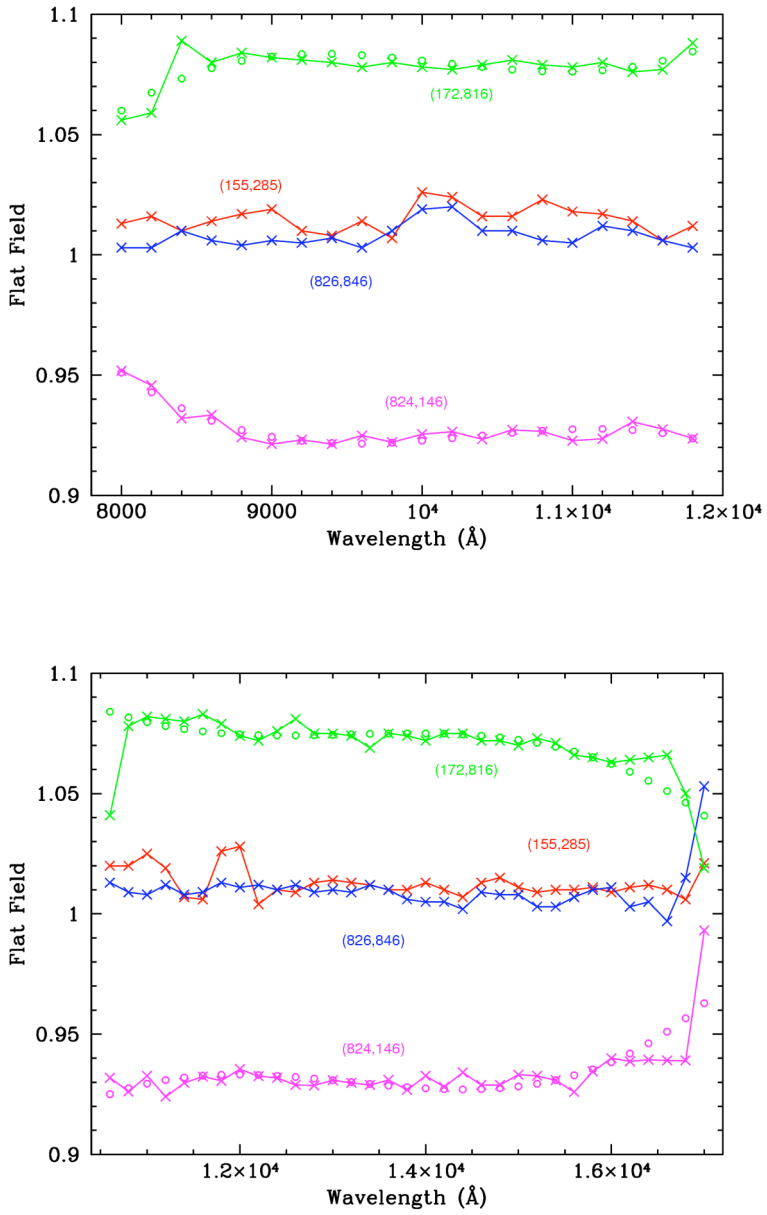

Figure 8: The variation of the flat-field as a function of wavelength for a few selected pixels. Each point refers to the mean value over nine pixels. The upper plot shows the behaviour for the G102 grism and the lower plot for G141. The coordinates of the pixels are indicated. The open circles (for the low pixel (magenta) and high pixel (green) values) are derived from the polynomial fit, which is stored in the flat-field cube.

5. Conclusions

This ISR presented the WFC3 IR grism calibrations carried out during thermal vacuum 2 (TV2). The grisms show linear dispersion relations and trace definitions, which vary across the field of view and can be well approximated by linear fits. The average dispersion is ~25 Å/pixel and ~47 Å/pixel for the G102 and G141 grisms, respectively. The new IR grisms show excellent design characteristics with more than 90% of the power in the first order. Peak efficiency of WFC3 with the G102 and G141 grisms reach ~31% and ~41%, respectively. The resulting configuration and sensitivity files were used in a simulation package (aXeSIM) for HST/WFC3 grism observations and are available from our Web pages (http://www.stecf.org). Aperture corrections are given for both grims as function of wavelength. Furthermore, we derive flat-field cubes that provide pixel-to-pixel information as function of wavelength to an accuracy of about 1%. These flat-field data is based on narrow band (100Å) illuminations of the full detector area in steps of 200Å. Updated sensitivity calibrations will be derived when data from TV3 (March – April 2008) with the new detectors becomes available.

References

Larsen, Bushouse, & Walsh, 2005, ST-ECF Instrument Science Report, WFC3-2005-07
Kümmel, Kuntschner, Walsh, 2007, ST-ECF Newsletter, 43, 8